Detection of SARS-CoV-2 with Solid-State CRISPR-Cas12a-Assisted Nanopores (SCAN)

Reza Nouri ¹, Yuqian Jiang ^{2,3}, Zifan Tang ¹, Xiaojun Lance Lian ^{2,3,4} and Weihua Guan ^{1,2,*}

¹ Department of Electrical Engineering, Pennsylvania State University, University Park, Pennsylvania 16802, United States

² Department of Biomedical Engineering, Pennsylvania State University, University Park, Pennsylvania 16802, United States

³ Huck Institutes of the Life Sciences, Pennsylvania State University, University Park, Pennsylvania 16802, United States

⁴ Department of Biology, Pennsylvania State University, University Park, Pennsylvania 16802, United States

*Correspondence: Weihua Guan (w.guan@psu.edu)

ABSTRACT

The outbreak of the SARS-CoV-2 caused the COVID-19 disease to spread globally. Specific

and sensitive detection of SARS-CoV-2 facilitates early intervention and prevents the disease from

spread. Here, we present a solid-state CRISPR-Cas12a-assisted nanopore (SCAN) sensing strategy

for the specific detection of SARS-CoV-2. We introduced a nanopore-sized counting method to

measure the cleavage ratio of reporters, which is used as a criterion for positive/negative

classification. A kinetic cleavage model was developed and validated to predict the reporter size

distributions. The model revealed the tradeoffs between sensitivity, turnaround time, and false-

positive rate of the SARS-CoV-2 SCAN. With a preamplification and 30 min of CRISPR Cas12a

assay, we achieved excellent specificity against other common human coronaviruses and a limit

of detection of 13.5 copies/µl (22.5 aM) of viral RNA at the 95% confidence level. These results

suggested that the SCAN could provide a rapid, sensitive and specific analysis of SARS-CoV-2.

KEYWORDS

CRISPR, Cas 12a, SARS-CoV-2, COVID-19, Nanopore

2

The coronavirus disease 19 (COVID-19) caused by the severe acute respiratory syndrome coronavirus 2 (SARS-CoV-2) is an ongoing pandemic throughout the world ¹⁻². To facilitate the management and containment of the disease, reliable, rapid, and accessible testing is required. While numerous diagnostic strategies such as sequencing ³⁻⁶ and antibody test ⁷⁻⁹ have been introduced for SARS-CoV-2 detection, nucleic acid testings (NAT), primarily quantitative realtime PCR with reverse transcription (RT-qPCR), are the current gold standards ¹⁰⁻¹¹. The recent development of the clustered regularly interspaced short palindromic repeats (CRISPR)-based methods started a new path towards molecular diagnosis 12. Particularly, the discovery of the collateral cleavage of Cas proteins such as Cas12 and Cas13 made it possible to translate the sequence-specific targeting to detectable signals. These discoveries have led to a variety of CRISPR-mediated biosensors ¹³⁻²¹. These CRISPR-based methods often incorporate an amplification process such as polymerase chain reaction (PCR) ²²⁻²³, loop-mediated isothermal amplification (LAMP) ²⁴, or recombinase polymerase amplification (RPA) ²⁵⁻²⁶ to enhance the starting molecule population ^{14, 27}. Amplification coupled CRISPR-Cas detection has been shown to be highly sensitive (as low as fM level ¹³⁻¹⁴) and highly specific (down to single-nucleotide level ²⁸⁻²⁹). Due to their outstanding sensing performances, CRISPR-based systems have been adopted for SARS-CoV-2 detection amid the ongoing COVID-19 pandemic ^{10, 23, 30-38}.

So far, most of the CRISPR-based methods use fluorescent, bioluminescent, or colorimetric reporters for readouts, which is easy to operate, sensitive and convenient ³⁹. As alternatives to the optical readout, electronic-based methods such as electrochemical ^{17, 40-42}, and field-effect ⁴³ have also been investigated due to their integration and miniaturization potential. One of the intriguing electronic readout systems utilized for CRISPR-based detection is the nanopore sensor ⁴⁴⁻⁴⁵. The single molecule sensitivity of the nanopore sensors has made them a promising candidate for

CRISPR-based detection. We previously demonstrated a solid-state CRISPR-Cas12a-assisted nanopore (SCAN) sensor for sequence-specific recognition of HIV-1 ⁴⁶. While we demonstrated that the SCAN can detect target DNA concentrations above 10 nM within an hour, detecting concentrations less than 10 nM with a fast turnaround time would likely require pre-amplification steps.

In this work, we developed a reverse transcription amplification coupled SCAN device for rapid, highly sensitive, and highly specific detection of SARS-CoV-2 viral RNAs. The method used an improved nanopore sized counting approach to examine the reporter size distributions and their relative abundance. We showed that the cleavage ratio of the intact circular ssDNA reporters could be quantified by the SCAN, which is used as a criterion for classifying the test as positive or negative. To guide the experiments, we developed a kinetic model to compute the reporter length distribution as a function of the cleavage reaction time. This experimentally validated model revealed the tradeoffs between sensitivity, turnaround time, and false-positive rate of the SARS-CoV-2 SCAN. With a preamplification and 30 min of CRISPR Cas12a assay, we achieve a limit of detection (LoD) of 13.5 copies/µl (22.5 aM) of SARS-CoV-2 viral RNA at the 95% confidence level. The SARS-CoV-2 SCAN has also shown excellent specificity against three other common human coronaviruses. Our results suggested that the SCAN could provide a rapid, sensitive, and specific analysis of SARS-CoV-2.

RESULTS AND DISCUSSION

Working principle of nanopore sized counting

Figure 1a illustrated the working scheme of the SARS-CoV-2 SCAN using nanopore sized counting. There were three streamlined steps: reverse transcription and amplification, Cas12 assay,

and nanopore-based molecule classification and counting. In the first step, a one-step reverse transcription-polymerase chain reaction (RT-PCR) of SARS-CoV-2 RNA was performed to improve the overall sensitivity of the system ^{31-32, 34}. After amplification, the complementary DNA (cDNA) amplicons were introduced to the sequence-specific CRISPR RNA (crRNA) and Cas12a ribonucleoprotein mixture (*a.k.a*, RNP). Upon the specific cDNA binding, the Cas12a could perform collateral cleavage on the surrounding ssDNA reporters ³⁹. We used circular M13mp18 single-stranded DNA (ssDNA) as the reporter in this study which is widely available and has an excellent signal-to-noise ratio in nanopore measurement. In the trans-cleavage process, the mother circular ssDNA reporters could be digested into daughter linear ssDNAs, and the daughter reporters could be further digested into granddaughter reporters (positive case in **Figure 1a**). On the other hand, if SARS-CoV-2 viral RNAs were not present in the analyte solutions, the Cas12a remains inactive and will not degrade the mother circular ssDNA reporter (negative case in **Figure 1a**).

These un-cleaved mother reporters and multi-generational cleaved daughter reporters were then counted and classified by a glass nanopore sensor to infer its size and concentration distribution. **Figure 1b** shows two representative ionic current time trace for a positive sample and a negative sample (no target control), using a glass nanopore with a diameter size less than 10 nm (**Figure S1a and b**). For the positive sample (presence of SARS-CoV-2 RNA), it is apparent that molecule translocation events become more frequent but have less current blockage magnitude as compared to the negative sample. This is because the mother circular reporters were cleaved to many smaller daughter linear reporters. Our previous work analyzed the resulting reporter concentration by nanopore digital counting without taking the daughter reporter size distribution into consideration ³⁰. This assumption is not exactly accurate if the reaction time is short. To further

analyze the daughter reporter size distribution and its relative abundance, we here adopted a nanopore sized counting method. First, the conventional event duration versus blockage was obtained from the ionic current time trace data (**Figure S1b**). As shown in **Figure 1c**, it is evident that the event duration and blockage in a positive case are smaller than in a negative case. Second, we classified each event based on its event charge deficit (ECD), which is used as the molecule size approximation⁴⁰. The ECD is defined as $ECD = \int_{event} \Delta I(t) dt \cong \Delta I \tau^{41}$, where ΔI and τ are the duration and blockage of each event, respectively. It was previously demonstrated that ECDs of DNA translocations with the same length are identical regardless of whether the molecules are in a linear, circular relaxed, or supercoiled form ⁴⁰. An ECD bin size of 20 fC was used in this study unless otherwise stated. Third, the event rate of each ECD sub-population was obtained by normalizing sub-population event numbers by the nanopore reading time (**Figure 1d**). This enables us to quantify the reporter sub-population concentration through $R = C_i \alpha N_A$, where N_A is the Avogadro constant, and α is usually referred to as the capture rate $^{42-45}$.

The mean (μ) and standard deviation (σ) of the ECD value in the negative cases was used to establish an ECD threshold ($ECDt=\mu-2\sigma$, dashed line in **Figure 1d**). An event must have an ECD larger than ECDt to be classified as the intact mother reporters (*i.e.*, to the right of the dashed line in **Figure 1d**). To quantify the percentage of the mother reporters being cleaved into daughter reporters, we defined the cleavage ratio (CR) as the ratio between the cleaved mother reporter ($C_0 - C_{uncleaved}$) to the total initial mother reporter (C_0). This cleavage ratio can be experimentally obtained by evaluating the aggregated event rate as

$$CR = 1 - \sum_{i} R_{vi} / \sum_{i} R_{ni} \tag{1}$$

in which the event rate summation is over all events with ECD larger than ECDt (thus representing

the intact mother reporter concentration in the system), and n and p denote the negative and positive cases, respectively. The increase in the cleavage ratio of a testing sample would confirm the existence of the target viral RNA.

SARS-CoV-2 Cas12a assay validation

Prior to the Cas12a assay, a one-step RT-PCR was performed to increase the number of molecules and boost the signal. We utilized the primers designed by the United States Centers for Disease Control and Prevention (CDC) targeting the N2 region of the SARS-CoV-2 ⁴⁶. We performed a real-time RT-PCR with 2×10⁵ copies/µl of SARS-CoV-2 viral RNAs for a duration of 45 cycles. The fluorescent signal confirmed the amplification after 20 cycles (**Figure S2**). To further confirm the amplicon product, we performed gel electrophoresis of the RT-PCR products, which showed a sharp band at 67 bp, as expected with our RT-PCT primer design (**Figure 2a**).

Afterward, we performed the SARS-CoV-2 specific Cas12a assay with reaction time ranging from 0 to 30 mins. The reaction was stopped by adding the DNA gel loading dye (6X), which contained ethylenediaminetetraacetic acid (EDTA). **Figure 2b** presents the gel electrophoresis results of the Cas12a assay. We observed several important features. First, the mother reporter appeared in a double band around 7 kbp. This is due to the fact that electrophoretic mobility of DNA in gels could also be affected by the conformation of the DNA⁴⁷. Second, the daughter reporters become visible after 2 minutes, indicating the cleavage of mother reporters. Third, the primers were observed as a blurred short band in all cases. Fourth, as we increased the reaction time, more mother reporters were cleaved. At 30 minutes, the 7.2 kilo-nucleotides (knt) band of un-cleaved mother ssDNA become barely visible.

To examine the Cas12a cleavage kinetics at a much longer time scale, we performed another

test by intentionally extending the Cas12a reaction time up to 24 hours. We found that all mother and prior generation daughter reporters were completely cleaved to be less than 250 nt after 24 hours (**Figure S3**). This suggests the trans-cleavage activities indiscriminately and continuously affect both the mother reporters and the partially cleaved daughter reporters. As a control, we also performed the Cas12a assay for no target samples to confirm that no degradation of the mother reporters would occur in the absence of SARS-CoV-2 amplicons (**Figure S4**).

Highly sensitive nanopore measurement of the cleavage ratio

After validating the Cas12a assay with gel electrophoresis, we set out to perform the SARS-CoV-2 detection with the glass nanopore. We performed the Cas12a assay with different reaction times from 0 to 30 minutes and recorded the reporter translocations through the nanopore under 400 mV bias (**Figure S5**). Note that in our glass nanopore measurement, DNAs with sizes less than 100 bp are often too small to be detected. Those significantly cleaved reporters with lengths less than 100 bp and RT-PCR amplicons (67 bp) could not contribute to the detected signals. In addition, in our previous study ⁴⁸, we showed that the other components in the assay, such as Cas12a proteins, do not create signals in the nanopore experiment. Therefore, all the signals in the nanopore measurements are caused by the reporters with a length above the detectable threshold (a few hundred nucleotides).

Figure 2c shows the extracted translocation dwell time versus ionic current blockage at each reaction time. A clear shift of the blockage-duration distribution was observed when increasing the reaction time, indicating the changing populations of differently sized reporters. To quantify the abundance of differently sized reporters, we used an ECD bin size of 20 fC to classify the events into different sub-populations and calculated its corresponding event rate. **Figure 2d** shows

the event rate distribution for all sub-populations. As shown, the event rate of larger ECDs (longer reporters) is reducing as the cleavage reaction goes, whereas the event rate of smaller ECDs (shorter reporters) is increasing. Since the concentration of the analyte could be quantified by the event rate in the nanopore experiment, these measurements give us the capability to quantify the relative abundance of differently sized reporters.

To quantify the cleavage ratio at different reaction times, we utilized the nanopore-sized counting method. The case at 0 min of reaction was considered as the negative case to establish the *ECD*₁. The cleavage ratio (*CR*) at each reaction time was then obtained by using **Eq. 1**. As shown in **Figure 2e**, the *CR* was at 0.12 after 1 minute of reaction and increased as increasing the reaction time. For instance, *CR* was measured as 0.92 at 30 minutes of reaction. As the reaction times increase, more daughter and granddaughter reporters would be created, which increases the possibility of multi-turn cleavage. Therefore, the cleavage ratio increases at a lower rate as we increase the reaction time. It is noteworthy that we were able to detect the cleavage activity after 1 minute in nanopore reading, whereas no cleavage was barely visible in the gel after 1 minute of reaction (**Figure 2b**). This indicates that the nanopore is a much more sensitive readout system for *CR* measurement.

Cleavage numerical modeling and validation

In order to guide our experiments for rapid and sensitive detection of the cleavage ratio using nanopore experiment, we sought to develop a model to estimate the distribution of reporter length over the trans-cleavage process. At the start of the reaction, we assumed that each mother reporter has an identical length of L_m . As the reaction starts, the reporters (including mother and daughter reporters) were randomly picked by the activated Cas12a. The probability that a reporter was

picked and cleaved by the Cas12a was proportional to its cross-sectional area R_g^2 , where R_g is the gyration radius of the DNA coil. It has been shown that the gyration radius of DNA is proportional to the square root of its length $(L^{1/2})^{42}$. Therefore, the longer the reporter was, the more chance that it was bounded to and cleaved by the Cas12a. The reporter was cut into two parts randomly. We assumed a normal distribution to model the cleavage position in a report. The velocity of the cleavage was modeled by $v(t) = k_{cat} \frac{[E_0][S(t)]}{K_M + [S(t)]}$, in which $[E_0]$ is the initial enzyme (activated Cas12a) concentration, [S(t)] is the substrate concentration (mother and daughter reporters), k_{cat} and K_M are the catalytic rate and the Michaelis constant, respectively. We used previous reported k_{cat} and K_M value of 0.6 (1/s), and 2.7×10^{-6} , respectively ⁴⁹. This model was numerically implemented in a customized MATLAB code (see Figure S6 for model flowchart and results).

In order to validate this numerical model for predicting the reporter size distribution after reaction, we performed the Cas12a assay at three enzyme concentrations (7.5, 15, and 30 nM) with reaction times ranging from 0 mins to 24 hours. **Figure 3a** presents the gel electrophoresis results. As expected, higher enzyme concentration indeed results in faster cleavage activity since the cleavage velocity is proportional to the enzyme concentration. We extracted the length distribution of the reporter from the gel images by measuring the normalized grayscale values using ImageJ software ⁵⁰⁻⁵¹. The normalized reporter length distributions were then overlaid with the results produced by our model. As shown in **Figure 3b**, shorter daughter reporters were produced at a fixed reaction time as enzyme concentration was increased. Also, both model and gel results showed that the mother reporters were cleaved entirely after 24 hours. The distribution of reporter length captured by our model is consistent with the gel electrophoresis results, which validates our model.

The tradeoff between sensitivity, reaction time, and false-positive rate

Since the cleavage ratio (CR) was used to distinguish a positive and a negative sample, we calculated the CR with the model-produced length distributions. The model-derived CR values were then compared with the nanopore-measured CR values using the sized counting method (Eq.1). We measured the CR at different enzyme concentrations (7.5, 15, and 30 nM) with ranging reaction times from 0 to 30 mins. As shown in Figure 4a, the model predicted CR values agree excellently with that measured by the nanopore.

With the capability to calculate the CR at varying activated Cas 12a and reaction time, we were able to estimate the sensitivity and turnaround time of the SCAN system at any given CR threshold (CR_i) for a positive call. **Figure 4b** presents the minimal required reaction time versus the activated Cas12a enzyme concentration. Note that the activated Cas12a enzyme concentration is equal to the smaller values between SARS-Cov-2 amplicons and non-activated Cas12a concentration in the system. As shown in **Figure 4b**, at any given CR_t for a positive call, there is a tradeoff between turnaround time and sensitivity. More reaction time was required when decreasing the activated Cas 12a enzyme concentration. For instance, at $CR_t = 0.1$, more than 45 mins will be required to detect 1 nM of amplicons, whereas 0.45 min is sufficient with 100 nM amplicons. On the other hand, while increasing the CR_t could help to reduce the false-positive rate, it would increase the required minimal reaction time at any given amplicon concentrations. In fact, the CR is proportional to the product of cleavage velocity and reaction time (T_r) , $CR = v T_r$. The cleavage velocity v is proportional to the activated Cas12a concentration C_{enzyme} as $v = \beta C_{enzyme}$. Therefore, one can see that $C_{enzyme} T_r/CR$ should equal to the constant coefficient β . This relationship suggests there is a tradeoff between sensitivity (C_{enzvme}), reaction time (T_r), and false-positive rate (CR). With a fixed C_{enzyme} , a higher CR (less false-positive) calls for a longer

reaction time T_r . With a fixed CR, reducing the C_{enzyme} (better sensitivity) also requires a longer reaction time T_r (longer turnaround). By coupling with a pre-amplification step, the C_{enzyme} can be effectively enhanced and thus significantly reduce the required T_r (turnaround time).

Analytical specificity and sensitivity of SARS-CoV-2 SCAN

We then went to evaluate the analytical sensitivity and specificity of SARS-CoV-2 SCAN. We used heat-inactivated SARS-CoV-2 RNA samples at different concentrations ranging from 2 to 200 copies/µl. In addition, three other human coronaviruses (229E, NL63, and OC43) with a concentration of 5×10⁵ copies/µl were used as the non-target negative controls to evaluate the specificity. 5 µl of each sample was firstly amplified by RT-PCR for 45 cycles (Figure S7). The product of the RT-PCR was added to 30 nM of non-activated Cas12a. The Cas12a cleavage assay was performed at 37°C for 30 min. Afterward, the nanopore sized counting was performed to determine the cleavage ratio. A positive/negative call was subsequently derived by comparing the obtained cleavage ratio with CR_t (dashed line in Figure 5a). The CR_t was defined in our experiment as $\mu_0+2\sigma_0$ (0.089), where μ_0 (0.054) and σ_0 (0.017) are the mean and standard deviation of the cleavage ratio obtained from no target controls (i.e., SARS-CoV-2 sample at zero concentrations). Figure 5a presents the cleavage ratios of all SARS-CoV-2 and non-target human coronaviruses samples. As shown, the cleavage ratios for all non-target human coronavirus samples (circle, diamond, and star symbols in Figure 5a) are less than CRt and were correctly classified as negatives. This confirmed that the SCAN sensor has an excellent specificity against SARS-CoV-2.

For the serially diluted SARS-CoV-2 samples (square symbols in **Figure 5a**), we found that concentrations higher than 15 copies/µl were classified correctly as positives since their cleavage

ratios are much larger than CR_1 . The high cleavage ratio in these samples indicates the majority of the mother reporters were cleaved after 30 min of reaction. On the other hand, we started to observe false negatives results in samples with concentrations lower than 15 copies/ μ l. For instance, 1 out of 5 samples at a concentration of 10 copies/ μ l and 4 out of 5 samples at 2 copies/ μ l were misclassified as negatives. To estimate the LoD of SARS-CoV-2 SCAN, we examined the hit rate at each different SARS-CoV-2 concentration. The hit rate is defined as the number of replicates with a detected outcome per the total number of replicates tested ⁵². As shown in **Figure 5b**, the hit rate started to roll off from 1 to 0.8 when the concentration decreased from 15 copies/ μ l to 10 copies/ μ l. We fitted the experimental hit rate data with a logistic curve (**Figure 5b**) ⁵³⁻⁵⁴. Based on the fitting curve, we estimated the LoD of SARS-CoV-2 SCAN as 13.5 copies/ μ l (22.5 aM) at the 95% confidence level.

CONCLUSIONS

In summary, we introduced and evaluated a sized counting method for nanopores-assisted CRISPR-Cas12a-based detection of SARS-CoV-2. A sized counting scheme for cleavage quantification of the reporters in the Cas12a assay was introduced by utilizing ECD values from the nanopore experiment. We found that the nanopore is a sensitive readout system to measure the cleavage ratios, a criterion used for positive or negative classification. A kinetic cleavage model was developed and experimentally validated to predict the reporter length distribution. This model revealed the tradeoffs between sensitivity, reaction time, and false-positive rate in the SARS-CoV-2 SCAN. These tradeoffs could be relaxed by coupling with pre-amplification steps. With a 25 min RT-PCR step, 30 min of CRISPR Cas12a assay, and 10 min of nanopore reading (65 min of assay-to-result time), we achieved a limit of detection of 13.5 copies/µl (22.5 aM) of viral RNA. The SARS-CoV-2 SCAN showed an excellent specificity with no cross-reactivity to other human

coronaviruses. These results suggested that the solid-state CRISPR -Cas12a-assisted nanopores

could provide a rapid, sensitive, and specific analysis of SARS-CoV-2.

ASSOCIATED CONTENT

The Supporting Information is available. Method section including materials and chemicals,

SARS-CoV-2 RT-PCR and Cas12a assay, glass nanopore fabrication and characterization, and

nanopore sensing and data analysis sections. Nanopore characterization and current drop-dwell

time measurements. Results of RT-qPCR. Gel electrophoresis results of the Cas12a assay products

at five reaction times from 0.5 to 24 hours. Gel electrophoresis results of the no target negative

control samples. Translocation recording of ssDNA reporters at different reaction times through

the glass nanopore. Algorithm and the model details for estimation of the reporter length

distribution over the trans-cleavage process. RT-PCR results for the analytical specificity and

sensitivity test (PDF).

AUTHOR INFORMATION

Corresponding Author

* Email: Weihua Guan (w.guan@psu.edu)

ORCID

Weihua Guan: 0000-0002-8435-9672

Xiaojun Lance Lian: 0000-0002-9161-1004

Author contributions

W.G. conceived the concept and together with X.L.L. supervised the study. R.N. and Z.T. designed

14

and performed the RT-PCR. R.N. and Y.J. developed and performed the Cas12a assay. R.N. performed the nanopore fabrication and sensing experiment. W.G. and R.N. co-wrote the manuscript, with discussion from all authors.

NOTES

The authors declare no competing financial interest.

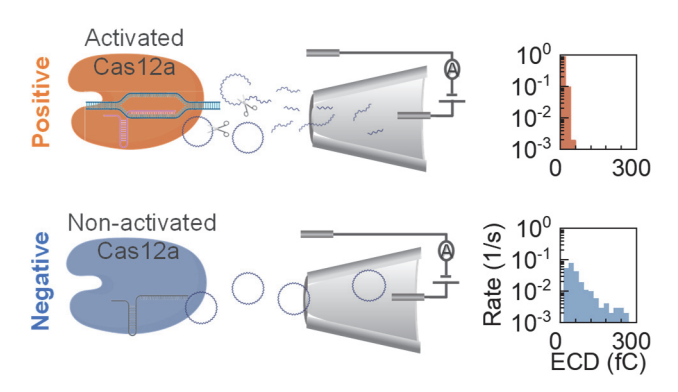
ACKNOWLEDGMENTS

This work is supported by the National Science Foundation under Grant No. 1710831, 1912410, 2045169. The content is solely the responsibility of the authors and does not necessarily represent the official views of the National Science Foundation. W. G acknowledges the support from Coronavirus Research Seed Fund from PennState Huck Institutes of the Life Sciences & Materials Research Institute.

FIGURES CAPTIONS

- **Figure 1**. a) Schematic of Solid-State CRISPR-Cas12a-Assisted Nanopore (SCAN) sensor. The process starts with a preamplification step, followed by CRISPR assay and nanopore analysis. In a Positive case (upper side), the trans-cleavage activity of the Cas12a after activation cause degradation of the circular ssDNA reporters, resulting in reduced reporter size. In a negative case, the Cas12a is not activated in the absence of target dsDNA, and thus the ssDNA reporters are not cleaved. b) Examples of a typical ionic current trace for a positive and negative case. c) Duration and blockage of translocation events for a positive and negative case. The lines represent equivalent ECD lines from 20 to 300 fC (with a bin size of 20 fC). e) Event rate distribution at different ECD values. The right side of the dashed line represents the un-cleaved region.
- **Figure 2.** a) Gel electrophoresis results of the RT-PCR products validating the length of amplicons as 67 bp. b) Gel electrophoresis results of Cas12a assay products at different reaction times from 0 to 30 minutes. In all cases, the non-activated Cas12a and reporter concentration was fixed as 30 nM and 2.1 nM, respectively. c) Current drop and dwell times of the ssDNA reporter translocation events at different reaction times through the glass nanopore under 400 mV bias. The buffer salt concentration was fixed as 1 M. The total number of events and nanopore reading time is shown for each case d) Event rate distribution at different ECD values. The area right to the dashed line represents the un-cleaved region. e) The calculated values for reporter cleavage ratios at different reaction times.
- **Figure 3**. a) Gel electrophoresis results of the Cas12a assay at three different initial enzyme concentrations (7.5, 15, and 30 nM) and different reaction times (from 0 minutes to 24 hours). b) Comparison between the reporter length distribution captured by the model and Gel electrophoresis. The normalized grayscale value of the gel results was measured by ImageJ software for the estimation of the reporter concentration.
- **Figure 4.** a) The measured cleavage ratio of the ssDNA reporter by the sized counting method (experiment) and the numerical model at different reaction times. The outcome of the model and nanopore experiment is in good agreement at three different enzyme concentrations (7.5, 15, and 30 nM). b) Required reaction time versus the activated Cas12a enzyme concentration (from 0.1 to 1000 nM) at four different *CR* thresholds values.
- **Figure 5.** a) Cleavage ratio of three different human coronaviruses samples (for specificity test) and SARS-CoV-2 (for sensitivity test) with different input RNA concentrations. Five repeats were performed for lower concentrations (less than 20 copies/μl), and three were tested for higher concentrations (more than 20 copies/μl) and non-target control samples. The cleavage ratios were measured using the nanopore sized counting experiment. The average and standard deviation of the *CR* values of 5 negative target controls were measured to identify the threshold for separating positive from negative calls. Any cases with a *CR* below $CR_t = \mu + 2\sigma$ (0.089) were classified as negatives. b) The hit rate percentage at different concentrations of SARS-CoV-2 RNA. The LoD was estimated as 13.5 copies/μl at a 95% confidence level.

TOC



REFERENCES

- 1. Zhou, P.; Yang, X.-L.; Wang, X.-G.; Hu, B.; Zhang, L.; Zhang, W.; Si, H.-R.; Zhu, Y.; Li, B.; Huang, C.-L., A pneumonia outbreak associated with a new coronavirus of probable bat origin. *nature* **2020**, *579* (7798), 270-273.
- 2. Zhu, N.; Zhang, D.; Wang, W.; Li, X.; Yang, B.; Song, J.; Zhao, X.; Huang, B.; Shi, W.; Lu, R., A novel coronavirus from patients with pneumonia in China, 2019. *New England journal of medicine* **2019**, *382*, 727-733.
- 3. Lu, R.; Zhao, X.; Li, J.; Niu, P.; Yang, B.; Wu, H.; Wang, W.; Song, H.; Huang, B.; Zhu, N., Genomic characterisation and epidemiology of 2019 novel coronavirus: implications for virus origins and receptor binding. *The lancet* **2020**, *395* (10224), 565-574.
- 4. Chiara, M.; D'Erchia, A. M.; Gissi, C.; Manzari, C.; Parisi, A.; Resta, N.; Zambelli, F.; Picardi, E.; Pavesi, G.; Horner, D. S., Next generation sequencing of SARS-CoV-2 genomes: challenges, applications and opportunities. *Briefings in Bioinformatics* **2021**, *22* (2), 616-630.
- 5. Aynaud, M.-M.; Hernandez, J. J.; Barutcu, S.; Braunschweig, U.; Chan, K.; Pearson, J. D.; Trcka, D.; Prosser, S. L.; Kim, J.; Barrios-Rodiles, M., A multiplexed, next generation sequencing platform for high-throughput detection of SARS-CoV-2. *Nature communications* **2021**, *12* (1), 1-10.
- 6. Bhoyar, R. C.; Jain, A.; Sehgal, P.; Divakar, M. K.; Sharma, D.; Imran, M.; Jolly, B.; Ranjan, G.; Rophina, M.; Sharma, S., High throughput detection and genetic epidemiology of SARS-CoV-2 using COVIDSeq next-generation sequencing. *PloS one* **2021**, *16* (2), e0247115.
- 7. Dzimianski, J. V.; Lorig-Roach, N.; O'Rourke, S. M.; Alexander, D. L.; Kimmey, J. M.; DuBois, R. M., Rapid and sensitive detection of SARS-CoV-2 antibodies by biolayer interferometry. *Scientific reports* **2020**, *10* (1), 1-12.
- 8. Meng, Q.-B.; Peng, J.-J.; Wei, X.; Yang, J.-Y.; Li, P.-C.; Qu, Z.-W.; Xiong, Y.-F.; Wu, G.-J.; Hu, Z.-M.; Yu, J.-C., Clinical application of combined detection of SARS-CoV-2-specific antibody and nucleic acid. *World journal of clinical cases* **2020**, *8* (19), 4360.
- 9. Petherick, A., Developing antibody tests for SARS-CoV-2. *The Lancet* **2020**, *395* (10230), 1101-1102.
- Udugama, B.; Kadhiresan, P.; Kozlowski, H. N.; Malekjahani, A.; Osborne, M.; Li, V. Y.; Chen, H.; Mubareka, S.; Gubbay, J. B.; Chan, W. C., Diagnosing COVID-19: the disease and tools for detection. ACS nano 2020, 14 (4), 3822-3835.
- 11. Jokela, P.; Jääskeläinen, A. E.; Jarva, H.; Holma, T.; Ahava, M. J.; Mannonen, L.; Lappalainen, M.; Kurkela, S.; Loginov, R., SARS-CoV-2 sample-to-answer nucleic acid testing in a tertiary care emergency department: evaluation and utility. *Journal of Clinical Virology* **2020**, *131*, 104614.
- 12. Doudna, J. A.; Charpentier, E., The new frontier of genome engineering with CRISPR-Cas9. *Science* **2014**, *346* (6213).
- 13. Gootenberg, J. S.; Abudayyeh, O. O.; Kellner, M. J.; Joung, J.; Collins, J. J.; Zhang, F., Multiplexed and portable nucleic acid detection platform with Cas13, Cas12a, and Csm6. *Science* **2018**, *360* (6387), 439-444.
- 14. Gootenberg, J. S.; Abudayyeh, O. O.; Lee, J. W.; Essletzbichler, P.; Dy, A. J.; Joung, J.; Verdine, V.; Donghia, N.; Daringer, N. M.; Freije, C. A., Nucleic acid detection with CRISPR-Cas13a/C2c2. *Science* **2017**, *356* (6336), 438-442.
- 15. Abudayyeh, O. O.; Gootenberg, J. S.; Kellner, M. J.; Zhang, F., Nucleic acid detection of plant genes using CRISPR-Cas13. *The CRISPR Journal* **2019**, *2* (3), 165-171.
- 16. Li, S.-Y.; Cheng, Q.-X.; Liu, J.-K.; Nie, X.-Q.; Zhao, G.-P.; Wang, J., CRISPR-Cas12a has both cisand trans-cleavage activities on single-stranded DNA. *Cell research* **2018**, *28* (4), 491-493.
- 17. Bruch, R.; Baaske, J.; Chatelle, C.; Meirich, M.; Madlener, S.; Weber, W.; Dincer, C.; Urban, G. A., CRISPR/Cas13a powered electrochemical microfluidic biosensor for nucleic acid amplification free miRNA diagnostics. *Advanced Materials* **2019**, *31* (51), 1905311.

- 18. Shao, N.; Han, X.; Song, Y.; Zhang, P.; Qin, L., CRISPR-Cas12a Coupled with Platinum Nanoreporter for Visual Quantification of SNVs on a Volumetric Bar-Chart Chip. *Analytical chemistry* **2019**, *91* (19), 12384-12391.
- 19. Li, L.; Li, S.; Wu, N.; Wu, J.; Wang, G.; Zhao, G.; Wang, J., HOLMESv2: a CRISPR-Cas12b-assisted platform for nucleic acid detection and DNA methylation quantitation. *ACS synthetic biology* **2019**, 8 (10), 2228-2237.
- 20. Qin, P.; Park, M.; Alfson, K. J.; Tamhankar, M.; Carrion, R.; Patterson, J. L.; Griffiths, A.; He, Q.; Yildiz, A.; Mathies, R., Rapid and fully microfluidic Ebola virus detection with CRISPR-Cas13a. *ACS sensors* **2019**, *4* (4), 1048-1054.
- 21. Kellner, M. J.; Koob, J. G.; Gootenberg, J. S.; Abudayyeh, O. O.; Zhang, F., SHERLOCK: nucleic acid detection with CRISPR nucleases. *Nature protocols* **2019**, *14* (10), 2986-3012.
- 22. Yuan, C.; Tian, T.; Sun, J.; Hu, M.; Wang, X.; Xiong, E.; Cheng, M.; Bao, Y.; Lin, W.; Jiang, J., Universal and naked-eye gene detection platform based on the clustered regularly interspaced short palindromic repeats/cas12a/13a system. *Analytical chemistry* **2020**, *92* (5), 4029-4037.
- 23. Rauch, J. N.; Valois, E.; Solley, S. C.; Braig, F.; Lach, R. S.; Audouard, M.; Ponce-Rojas, J. C.; Costello, M. S.; Baxter, N. J.; Kosik, K. S., A scalable, easy-to-deploy protocol for Cas13-based detection of SARS-CoV-2 genetic material. *Journal of clinical microbiology* **2021**, *59* (4), e02402-20.
- 24. Qian, C.; Wu, H.; Shi, Y.; Wu, J.; Chen, H., Dehydrated CRISPR-mediated DNA analysis for visualized animal-borne virus sensing in the unprocessed blood sample. *Sensors and Actuators B: Chemical* **2020**, *305*, 127440.
- 25. Chenot, C. c.; Robiette, R. l.; Collin, S., First evidence of the cysteine and glutathione conjugates of 3-sulfanylpentan-1-ol in hop (Humulus lupulus L.). *Journal of agricultural and food chemistry* **2019**, 67 (14), 4002-4010.
- 26. Sullivan, T. J.; Dhar, A. K.; Cruz-Flores, R.; Bodnar, A. G., Rapid, CRISPR-based, field-deployable detection of white spot syndrome virus in shrimp. *Scientific reports* **2019**, *9* (1), 1-7.
- 27. Abudayyeh, O. O.; Gootenberg, J. S.; Konermann, S.; Joung, J.; Slaymaker, I. M.; Cox, D. B.; Shmakov, S.; Makarova, K. S.; Semenova, E.; Minakhin, L., C2c2 is a single-component programmable RNA-guided RNA-targeting CRISPR effector. *Science* **2016**, *353* (6299), 5573.
- 28. Patchsung, M.; Jantarug, K.; Pattama, A.; Aphicho, K.; Suraritdechachai, S.; Meesawat, P.; Sappakhaw, K.; Leelahakorn, N.; Ruenkam, T.; Wongsatit, T., Clinical validation of a Cas13-based assay for the detection of SARS-CoV-2 RNA. *Nature Biomedical Engineering* **2020**, *4* (12), 1140-1149.
- 29. Harrington, L. B.; Burstein, D.; Chen, J. S.; Paez-Espino, D.; Ma, E.; Witte, I. P.; Cofsky, J. C.; Kyrpides, N. C.; Banfield, J. F.; Doudna, J. A., Programmed DNA destruction by miniature CRISPR-Cas14 enzymes. *Science* **2018**, *362* (6416), 839-842.
- 30. Nouri, R.; Tang, Z.; Dong, M.; Liu, T.; Kshirsagar, A.; Guan, W., CRISPR-based detection of SARS-CoV-2: A review from sample to result. *Biosensors and Bioelectronics* **2021**, *178*, 113012.
- 31. Broughton, J. P.; Deng, X.; Yu, G.; Fasching, C. L.; Servellita, V.; Singh, J.; Miao, X.; Streithorst, J. A.; Granados, A.; Sotomayor-Gonzalez, A.; Zorn, K.; Gopez, A.; Hsu, E.; Gu, W.; Miller, S.; Pan, C.-Y.; Guevara, H.; Wadford, D. A.; Chen, J. S.; Chiu, C. Y., CRISPR–Cas12-based detection of SARS-CoV-2. *Nature Biotechnology* **2020**, *38* (7), 870-874.
- 32. Ali, Z.; Aman, R.; Mahas, A.; Rao, G. S.; Tehseen, M.; Marsic, T.; Salunke, R.; Subudhi, A. K.; Hala, S. M.; Hamdan, S. M., iSCAN: An RT-LAMP-coupled CRISPR-Cas12 module for rapid, sensitive detection of SARS-CoV-2. *Virus research* **2020**, *288*, 198129.
- 33. Ding, X.; Yin, K.; Li, Z.; Lalla, R. V.; Ballesteros, E.; Sfeir, M. M.; Liu, C., Ultrasensitive and visual detection of SARS-CoV-2 using all-in-one dual CRISPR-Cas12a assay. *Nature communications* **2020**, *11* (1), 1-10.
- 34. Guo, L.; Sun, X.; Wang, X.; Liang, C.; Jiang, H.; Gao, Q.; Dai, M.; Qu, B.; Fang, S.; Mao, Y., SARS-CoV-2 detection with CRISPR diagnostics. *Cell discovery* **2020**, *6* (1), 1-4.

- 35. Arizti-Sanz, J.; Freije, C. A.; Stanton, A. C.; Petros, B. A.; Boehm, C. K.; Siddiqui, S.; Shaw, B. M.; Adams, G.; Kosoko-Thoroddsen, T.-S. F.; Kemball, M. E., Streamlined inactivation, amplification, and Cas13-based detection of SARS-CoV-2. *Nature communications* **2020**, *11* (1), 1-9.
- 36. Abbott, T. R.; Dhamdhere, G.; Liu, Y.; Lin, X.; Goudy, L.; Zeng, L.; Chemparathy, A.; Chmura, S.; Heaton, N. S.; Debs, R., Development of CRISPR as an antiviral strategy to combat SARS-CoV-2 and influenza. *Cell* **2020**, *181* (4), 865-876. e12.
- 37. Wang, R.; Qian, C.; Pang, Y.; Li, M.; Yang, Y.; Ma, H.; Zhao, M.; Qian, F.; Yu, H.; Liu, Z., opvCRISPR: One-pot visual RT-LAMP-CRISPR platform for SARS-cov-2 detection. *Biosensors and Bioelectronics* **2021**, *172*, 112766.
- 38. Ning, B.; Yu, T.; Zhang, S.; Huang, Z.; Tian, D.; Lin, Z.; Niu, A.; Golden, N.; Hensley, K.; Threeton, B., A smartphone-read ultrasensitive and quantitative saliva test for COVID-19. *Science advances* **2021**, *7* (2), eabe3703.
- 39. Chen, J. S.; Ma, E.; Harrington, L. B.; Da Costa, M.; Tian, X.; Palefsky, J. M.; Doudna, J. A., CRISPR-Cas12a target binding unleashes indiscriminate single-stranded DNase activity. *Science* **2018**, *360* (6387), 436-439.
- 40. Fologea, D.; Brandin, E.; Uplinger, J.; Branton, D.; Li, J., DNA conformation and base number simultaneously determined in a nanopore. *Electrophoresis* **2007**, *28* (18), 3186-3192.
- 41. Fologea, D.; Gershow, M.; Ledden, B.; McNabb, D. S.; Golovchenko, J. A.; Li, J., Detecting single stranded DNA with a solid state nanopore. *Nano letters* **2005**, *5* (10), 1905-1909.
- 42. Grosberg, A. Y.; Rabin, Y., DNA capture into a nanopore: interplay of diffusion and electrohydrodynamics. *The Journal of chemical physics* **2010**, *133* (16), 10B617.
- 43. Albrecht, T., Single-molecule analysis with solid-state nanopores. *Annual Review of Analytical Chemistry* **2019**, *12*, 371-387.
- 44. Wanunu, M.; Sutin, J.; McNally, B.; Chow, A.; Meller, A., DNA translocation governed by interactions with solid-state nanopores. *Biophysical journal* **2008**, *95* (10), 4716-4725.
- 45. Nouri, R.; Tang, Z.; Guan, W., Calibration-free nanopore digital counting of single molecules. *Analytical chemistry* **2019**, *91* (17), 11178-11184.
- 46. Lu, X.; Wang, L.; Sakthivel, S. K.; Whitaker, B.; Murray, J.; Kamili, S.; Lynch, B.; Malapati, L.; Burke, S. A.; Harcourt, J., US CDC real-time reverse transcription PCR panel for detection of severe acute respiratory syndrome coronavirus 2. *Emerging infectious diseases* **2020**, *26* (8), 1654.
- 47. Duke, T.; Viovy, J. L.; Semenov, A. N., Electrophoretic mobility of DNA in gels. I. New biased reptation theory including fluctuations. *Biopolymers: Original Research on Biomolecules* **1994**, *34* (2), 239-247.
- 48. Nouri, R.; Jiang, Y.; Lian, X. L.; Guan, W., Sequence-specific recognition of HIV-1 DNA with solid-state CRISPR-Cas12a-assisted nanopores (SCAN). *ACS sensors* **2020**, *5* (5), 1273-1280.
- 49. Ramachandran, A.; Santiago, J. G., CRISPR Enzyme Kinetics for Molecular Diagnostics. *Analytical Chemistry* **2021**, *93* (20), 7456–7464.
- 50. Alonso Villela, S. M.; Kraiem, H.; Bouhaouala Zahar, B.; Bideaux, C.; Aceves Lara, C. A.; Fillaudeau, L., A protocol for recombinant protein quantification by densitometry. *MicrobiologyOpen* **2020**, *9* (6), 1175-1182.
- 51. McKenzie, B.; Kay, G.; Matthews, K. H.; Knott, R. M.; Cairns, D., The hen's egg chorioallantoic membrane (HET-CAM) test to predict the ophthalmic irritation potential of a cysteamine-containing gel: Quantification using Photoshop® and ImageJ. *International journal of pharmaceutics* **2015**, *490* (1-2), 1-8.
- 52. Benschop, K.; Molenkamp, R.; van der Ham, A.; Wolthers, K.; Beld, M., Rapid detection of human parechoviruses in clinical samples by real-time PCR. *Journal of Clinical Virology* **2008**, *41* (2), 69-74.
- 53. Holstein, C. A.; Griffin, M.; Hong, J.; Sampson, P. D., Statistical method for determining and comparing limits of detection of bioassays. *Analytical chemistry* **2015**, *87* (19), 9795-9801.
- 54. Forootan, A.; Sjöback, R.; Björkman, J.; Sjögreen, B.; Linz, L.; Kubista, M., Methods to determine

limit of detection and limit of quantification in quantitative real-time PCR (qPCR). Biomolecular detection and quantification 2017, 12, 1-6.